WILEY-VCH

DOI: 10.1002/smll.201804267

Article type: Full paper

Mechanisms of Self-assembly and Energy Harvesting in Tuneable Conjugates of Quantum Dots and Engineered Photovoltaic Proteins

*Juntai Liu, Judith Mantell, Natalie di Bartolo and Michael R. Jones**

Juntai Liu, Dr. Natalie di Bartolo, Dr. Michael R. Jones

School of Biochemistry, Biomedical Sciences Building, University of Bristol, University Walk, Bristol BS8 1TD, United Kingdom.

E-mail: m.r.jones@bristol.ac.uk

Judith Mantell

Wolfson Bioimaging Facility, Biomedical Sciences Building, University of Bristol, University Walk, Bristol BS8 1TD, United Kingdom.

Keywords: biohybrid, self-assembly, reaction centers, quantum dots, photosynthesis;

ABSTRACT

Photoreaction centers facilitate the solar energy conversion at the heart of photosynthesis and there is increasing interest in their incorporation into biohybrid devices for solar energy conversion, sensing and other applications. In this work we describe the self-assembly of conjugates between engineered bacterial reaction centers (RCs) and quantum dots (QDs) that act as a synthetic light harvesting system. The interface between protein and QD is provided by a poly-histidine tag that confers a tight and specific binding and defines the geometry of the interaction. Protein engineering that changes the pigment composition of the RC is used to identify Förster resonance energy transfer (FRET) as the mechanism through which QDs can drive RC photochemistry with a high energy transfer efficiency. We provide a thermodynamic explanation of RC/QD conjugation based on a multiple/independent binding model. We also demonstrate that the presence of multiple binding sites affects energy coupling not only between RCs and QDs but also among the bound RCs themselves, effects which likely stem from restricted RC dynamics at the QD surface in denser conjugates. These findings are readily transferrable to many other conjugate systems between proteins or combinations of proteins and other nano-materials.

1. Introduction

Reaction centers (RCs) are integral membrane pigment-proteins responsible for the transduction of sunlight into biochemical energy in photosynthesis.[1–3] The key step of this energy conversion is the highly quantum-efficient separation of electrical charge between opposite poles of the RC protein (**Figure 1**a,b). The energy transducing functionality of natural photoreaction centers and related photosynthetic complexes/pigments is of interest to diverse alternative solar energy technologies including photoelectrochemical cells,[4–13] biosensing,[14,15] photosensing,[16]

molecular electronics[7] and solar fuel synthesis.[17–19] Studies have focused in the main on Photosystem I from cyanobacteria[20–22] and the RC and RC-LH1 complexes from purple photosynthetic bacteria such as *Rhodobacter* (*Rba.*) *sphaeroides*[23–26] (Figure 1a,b). This latter organism is a popular source of photoproteins because it is possible to apply extensive protein engineering to its well-characterised RC, enabling high-yield expression and purification of proteins with specifically-tailored properties or substantial modifications.

A feature of natural photosystems is selective harvesting of certain regions of the solar spectrum, the most obvious illustration being the predominant green colour of plant photosynthetic tissues that arises from relatively strong absorbance of red and blue light by chlorophyll and carotenoid pigments. As *Rba. sphaeroides* synthesises bacteriochlorophyll (BChl) as its primary photosynthetic pigment its RC exhibits strong absorbance in the near-infrared between 700 and 950 nm, and in the near-UV below 420 nm, but its absorbance across the visible region is relatively weak (Figure 1c). A limitation in the use of this protein in device technologies is therefore sub-optimal harvesting of light energy across much of the region where the solar radiation at the earth's surface is maximal,[27] and this limitation is manifest in action spectra of photocurrent density in photoelectrochemical cells based on *Rba. sphaeroides* pigment-proteins.[28–33]

In this study we investigated directed self-assembly of conjugates between genetically-engineered *Rba. sphaeroides* RCs and water-soluble cadmium telluride (CdTe) quantum dots (QDs). The tuneable optical properties of these semiconductor nanocrystals have been exploited in a variety of technologies including solar cells and diverse biological applications.[34–36] The particular QDs employed in the present work have broad absorbance across the visible spectrum and an emission band centered at 750 nm that overlaps with RC absorbance bands centered at 760 nm and 800 nm (Figure 1c). These QDs therefore were capable of acting as a synthetic light

harvesting system for energy transfer[37,38] and charge separation[23–26] in the *Rba. sphaeroides* RC (Figure 1b).

Through the use of cofactor-modified proteins we identify the mechanism of energy transfer between photo-excited QDs and bound RCs as Förster resonance energy transfer (FRET)[39–42] and develop a detailed thermodynamic description of self-directed binding between RCs and QDs based on a multiple/independent binding model[43]. As QDs have a high surface-to-volume ratio, and any portion of the surface can act as a binding site, QDs could accommodate multiple RCs and hence energy capture could be tuned up to a 92 % efficiency by varying the ratio of RCs to QDs in the assembled conjugates. Increasing the density of RCs surrounding each QD also enhanced the single donor-acceptor FRET efficiency, probably as a result of constraining RC motion. In conjugates formed between a cofactor-modified RC and QDs, increasing the RC density also caused the appearance of a new energy quenching pathway, suggesting that controlling protein density can also be used as a way of switching functionality. Our insights into the mechanism of nano-conjugate assembly are readily transferrable to other biohybrid systems that can be self-assembled from a wider range of adapted proteins or combinations of proteins with nanomaterials such as metal nanoparticles or carbon dots.

2. Results

2.1. Mechanism of binding of RCs to QDs.

Sucrose gradient ultracentrifugation was used to investigate the mechanism of binding of WT RCs to 750 nm-emitting water-soluble CdTe QDs (**Figure 2**a). In single component samples, QDs migrated to the 25/60 % interface in the lower part of a two-step sucrose gradient, whereas RCs remained at the upper 0/25 % interface. When RCs and QDs were mixed in a 10:1 ratio, ~95 % of

RCs were pulled down to the lower interface only when modified with a His_{10}-tag (Figure 2a). Henceforth WT RCs modified with a His-tag are denoted WT_H.

The conclusion that RC/QD binding was mediated by the protein His-tag was supported by the finding that WT RCs quenched QD emission only when His-tagged (Figure 2b; Figure S1a, Supporting Information). Measurements taken over extended time periods showed that this quenching was due to a stable association with His-tagged WT_H RCs at all RC:QD ratios tested (Figure S1b, Supporting Information). Quenching could be reversed by addition of imidazole or histidine, but not by NaCl (not shown). Cleavage of the His-tag using thrombin also produced recovery of QD emission that was dependent on the extent of cleavage (Figure S1c, Supporting Information).

The finding that quenching of QD emission could be reversed by SDS/heat treatment of RC/QD conjugates (Figure S1c, Supporting Information) indicated that it required the presence of intact RCs, and further suggested that it was not due to a change in the surface chemistry of the QDs caused by binding of the His-tag. To investigate this latter point further, QDs were incubated with two other His-tagged proteins, $XylE_H$, a xylose:proton symport membrane protein, and water-soluble $eGFP_H$. Neither produced a decrease in QD emission up to a 10:1 protein:QD ratio (Figure S1d, Supporting Information).

In addition to decreasing in intensity, it was noticeable that the maximum of the QD emission band blue-shifted somewhat as the RC:QD ratio increased (by a maximum of ~10 nm) (Figure S1a, Supporting Information). As preparations of QDs are expected to have a distribution of diameters around a certain mean, and hence a distribution of individual emission maxima, a possible explanation is that larger, “red-most” QDs are more effectively quenched by bound RCs due to a better spectral overlap with the RC absorption spectrum. Such a conclusion would be in accord

with quenching being due to FRET between the 750 nm emitting QDs and the near-IR absorbing RCs.

2.2. Conjugation to QDs enhances RC charge separation.

Proof of FRET between a donor and acceptor typically comprises decreased donor emission accompanied by increased acceptor emission, but in the present case the WT RC is barely fluorescent because excited state energy produces charge separation within a few picoseconds of arrival in the RC. This changes the absorbance spectrum of the RC however, and so it is possible to provide evidence in support of FRET from a QD to a RC by detecting charge separation enhancement in the RC when the attached QD is excited.

Absorbance spectroscopy was used to monitor changes in RC absorbance at 870 nm, associated with photo-oxidation of the primary electron donor (P) BChls (Figure 1b), in response to QD excitation. Excitation at 450 nm was used as the WT RC has a relatively low absorbance at this wavelength whereas the absorbance of QDs is relatively high (Figure 1c). To further reduce RC absorbance at this wavelength an engineered RC with a glycine to leucine replacement at residue 71 of the M-polypeptide (denoted GM71L) was also used.[44] This structural change prevents incorporation of the single RC carotenoid cofactor (see Figure 1b), markedly lowering RC absorbance at 450 nm due to loss of the broad Crt absorbance band between 420 and 580 nm (**Figure 3**a), but does not affect RC charge separation.[44]

Photobleaching of P at 870 nm was studied in WT and GM71L RCs with and without a His-tag and in the presence and absence of QDs (RC:QD ratio of 2.5). RCs were excited at 450 nm for seven seconds and averaged traces were fitted assuming a simple P/P^+ interconversion (see **Equation 1** in Experimental Procedures). Key fits are compared in Figure 3b, with all data and

fits in Figure S2, Supporting Information. In the absence of QDs the GM71L RCs showed less photobleaching than WT RCs due to their lower absorbance at 450 nm, with no significant differences in the extent of photobleaching between His-tagged and non-His-tagged RCs (top half of Figure S2, Supporting Information). Addition of QDs to non-His-tagged RCs did not change the extent of photobleaching significantly, consistent with a lack of binding (right column in Figure S2, Supporting Information). In contrast, adding QDs to His-tagged WT_H or $GM71L_H$ RCs produced marked increases in photobleaching relative to a control comprising RCs lacking a His-tag, amounting to a 2.4-fold increase for WT_H RCs over WT RCs, and a 3.1-fold increase for $GM71L_H$ RCs over GM71L RCs (Figure 3b). This trend was also seen in the rate constants for P photo-oxidation (k_f) deduced from the fits (Figure 3c)**.** These data indicated that energy is indeed donated from photo-excited QDs to bound His-tagged RCs and is used for charge separation, the QDs forming a synthetic antenna complex to complement RC light harvesting in a region of weak absorption.

A much stronger bleaching of the RC P band was induced by white light excitation of conjugates formed from different ratios of WT_H RCs and QDs. The dark recovery phase following 0.5 s of photoexcitation could be fitted using a single exponential with a lifetime in the region of ~1.1 s that did not vary significantly between different mixtures of RCs and QDs (Figure S3; Figure S4, Supporting Information). This showed that the recombination of $P^+Q_B^-$ was not affected by the presence of the QDs, suggesting a lack of electron or hole transfer between the two when the RC is in a metastable charge-separated state.

2.3. Energy can be transferred from QDs to photochemically-inactive RCs.

An alternative approach to demonstrating energy transfer between QDs and bound RCs is to engineer the RC to be fluorescent through of replacement of the valine residue at position 157 of the L subunit by arginine (VL157R).[45] This mutation reduces the occupancy of the P dimer binding site to ~0.5 BChls per RC, with complete loss of the P absorption band at 870 nm (**Figure 4**a), but has only small effects on the absorbance properties of the remaining monomeric BChl and BPhe cofactors and so the spectral overlap with QD emission. Photo-excitation of these remaining cofactors produces a weak emission band with a maximum at 801 nm, attributable to the monomeric BChls (absorbance band maximum at 798 nm), and a shoulder at 760 nm consistent with a smaller amount of emission from the BPhes (Figure 4a, red). Stable charge separation does not occur in the VL157R RC due to the absence of P, measurements by Jackson and co-workers showing that excitation of the monomeric BChls produces emission that decays over a period of several ns, with no indication of the formation of charge separated states such as $B_A^+H_A^-$ or $B_A^+Q_A^-$ [45].

Titration of QD emission using $VL157R_H$ RCs produced a similar quenching curve to that obtained with WT_H RCs (Figure 4b, purple), but the spectra included an additional $VL157R_H$ RC emission band that could be resolved by spectral deconvolution (Figure S5, Supporting Information). This demonstrated that quenching of QD emission was independent of the ability of the RC to form metastable cation or anion states such as P^+, H_A^- or Q_A^-. This finding strongly supports a FRET mechanism for QD quenching as opposed to a mechanism requiring electron transfer to or from the RC.

Comparison of the intensity of weak $VL157R_H$ emission in the absence and presence of QDs showed an interesting effect. As expected, in the absence of QDs the intensity of 801 nm emission from the $VL157R_H$ RC following excitation of its BPhe cofactors at 532 nm was linearly dependent

on protein concentration (Figure 4b, red). For VL157R_H/QD conjugates a greater amount of RC emission was seen at lower RC:QD ratios (Figure 4b, cyan compared with red), as might be expected if QDs also excited by the 532 nm light pass energy to bound RCs. However, the difference in VL157R_H RC emission intensity between the conjugate and the corresponding protein-only control was maximal at a RC:QD ratio of 2.5 and then decreased at higher ratios (Figure 4b, light orange) despite the extent of quenching of QD emission continuing to increase (Figure 4b, purple). The emission from 10:1 conjugates was slightly lower than the equivalent VL157R_H RC-only control (compare red and cyan traces in Figure 4b). This decline in VL157R_H fluorescence at higher RC:QD ratios was not due to self-shading, as the intensity of the 800 nm emission from the VL157R_H RCs in conjugates formed in a 10:1 RC:QD mix was linear with the absorbance of the conjugate (Figure S6a, Supporting Information). In addition, the effect was seen across a range of conjugate concentrations and was linear with concentration (Figure S6b, Supporting Information). The absorbance spectrum of the VL157R_H RC showed no variance across the range of conjugates formed (Figure S6c-d, Supporting Information), indicating that this effect was unlikely to be due to structural changes to the VL157R_H RC itself.

A feasible explanation for this effect is cross-relaxation between excited VL157R_H RCs as the number bound to each QD increases. Within the nanosecond scale life-time of the excited state formed by direct excitation of the VL157R_H RC, or by energy transfer from a QD (10% ~ 20% of the population was excited assuming one exciton was generated per absorbed photon), there is the possibility that an exciton can transfer between RCs and relax via a non-radiative pathway such as singlet-singlet annihilation (Figure 4c). As such a mechanism requires proximity of excitons, increasing the packing of RCs around each QD makes annihilation more likely, such that the

relative amount of emission declines. This effect was not seen for equivalent concentrations of VL157R_H RCs in the absence of QDs because they were free to diffuse independently in solution.

2.4. QD emission quenching is sensitive to spectral overlap.

Protein engineering can also be used to change the cofactor composition of the RC in a way that does not abolish photochemical charge separation. Mutations LM214H and LL185H are known to cause replacement of a BPhe by a BChl at the H_A or H_B cofactor binding site, respectively,[46,47] whilst the double mutation LM214H/LL185H causes both BPhes to be replaced by BChls. This cofactor change causes the Q_y absorbance band of the H_A and/or H_B cofactor to shift to longer wavelengths (**Figure 5**a), changing the profile of the region of spectral overlap between the RC and QD. The LM214H mutation slows the rate of charge separation by around two-fold and reduces its quantum yield to ~60 % due to replacement of the H_A BPhe by BChl.[46] In contrast the symmetrical LL185H mutation has no discernible effect on charge separation.[47]

Extinction coefficients for His-tagged versions of these three cofactor-exchange RCs were deduced by normalizing their absorption spectra to that of the WT_H RC using the P Q_y band in fully reduced RCs, as the intensity and shape of this band was interfered with least by the mutations (Figure 5a). The calculated spectral overlap was increased by between 20 % and 32 % (Figure 5b), and in accord with this the three mutants exerted slightly greater quenching of QD emission than the WT_H RC across the range of RC:QD ratios (Figure 5c). This sensitivity to spectral overlap was further evidence for the mechanism of QD emission quenching being FRET to the RC.

2.5. The morphology of RC/QD conjugates.

To investigate morphology, 10:1 RC/QD conjugates constructed with WT_H RCs were examined by transmission electron microscopy (TEM). Fast removal of buffer and transfer kept

the grid wet to mitigate against drying-induced aggregation prior to fixing with 3% uranyl acetate, the aim being to obtain images that were close representations of the state of the conjugates in solution. Recorded images revealed mostly lightly-stained objects that were evenly distributed in the field of view (**Figure 6**a), suggesting RC/QD conjugates were present as dispersed objects in solution. Images (Figure S7, Supporting Information) were analysed as described in Experimental Procedures, and compiled data on object diameter were fitted with a lognormal distribution with a mode at ~21.4 ± 1.0 nm **(**Figure 6b). This was a physically realistic dimension for an object comprising a shell of RCs surrounding a central QD. Because each RC was connected to its His-tag by a 16 amino acid flexible linker, the maximal theoretical distance between the surface of a QD and a bound RC should be around 6.1 nm, assuming that a fully extended polypeptide chain has a length of 0.38 nm per amino acid [48]. Therefore, the physically plausible range of diameters for a conjugate formed by a QD and multiple RCs should be between a maximum of ~32.7 nm and a minimum of ~20.5 nm based on expected mean diameters for QDs and RCs of 6.5 nm and 7.0 nm, respectively. The fitted distribution was at the low end of this theoretical range (Figure 6b), suggesting a closely packed structure.

Conjugate morphology was also examined by dynamic light scattering (DLS). Scattering profiles did not provide evidence of significant amounts of large-scale aggregate supporting the conclusion from TEM that conjugates were largely dispersed in solution. The measured hydrodynamic diameter for 10:1 RC/QD conjugates was 28.4 ± 0.7 nm (Figure 6c), again within the theoretical range but larger than the estimate from TEM. The hydrodynamic diameter generally decreased at RC:QD ratios below 5 indicating a transition in RC/QD conjugate population from particles with multiple RCs to particles that differed in their diameter by the height of one protein. A difference between mean diameters for 10:1 RC/QD conjugates derived from DLS and TEM

was not surprising, as DLS measures the diffusion coefficient of particles and hydrodynamic diameters are generally larger than actual size due to the presence of a solvent shell that migrates with the particle. In contrast negative stain TEM images particles without a water shell adsorbed on a surface. In the present case transient drying during sample preparation could have induced RCs to collapse onto the QDs, leading to an underestimation of the true particle size in solution, whereas the DLS data produced an overestimate of the true particle size due to the effect of the water shell.

2.6. Heterogeneity of actual RC:QD stoichiometry.

For any given mixture of His-tagged RCs and QDs, heterogeneity is expected in the actual RC:QD ratio for individual conjugates because multiple RCs can be accommodated by each QD and binding is a random process. As an understanding of the nature of this heterogeneity in RC:QD stoichiometry was important for an estimation of the efficiency of FRET, the interaction between His-tagged RCs and QDs was simulated using a model in which proteins could bind to multiple equivalent and independent sites on the surface of a QD (**Figure 7**a). The model is described by **Equation 2** in Experimental Procedures, where $\tilde{n}$ is the mean of the maximum number of RCs that can bind to a QD in any mixture (as this maximum number is actually a distribution of values rather than a fixed integer, as there are no discrete binding sites on the surface of a QD), k_{micro} is the microscopic association constant, and $\tilde{v}$ is the measured average RC:QD stoichiometry in any mixture.

To apply Equation 2, the average binding ratio for 10:1, 5:1, 2.5:1, 1.25:1 and 0.625:1 mixtures of WT_H RCs and QDs was determined by separating RC/QD conjugates and free RCs by ultracentrifugation on two-step 0 %/25 %/60 % sucrose density gradients (Figure S8a, Supporting

Information). Careful fractionation of these gradients followed by absorbance spectroscopy revealed that almost all of the protein was pulled to the 25 %/60 % interface due to being bound to a QD. To correct for continuing dissociation of bound RCs from conjugates during migration to the 25 %/60 % interface, the proportion of RCs bound to QDs in the initial mixture was calculated by summing the RC contents of fractions 1-8 (i.e. from the bottom of the gradient to just below the 0 %/25 % interface at the top of the gradient. The (minor) fraction of "free" RCs in the initial mixture remained at the 0 %/25 % interface (Fraction 9 and 10). SDS-PAGE/Western blot analysis of fractions from the 0 %/25 % interface using an anti-His antibody revealed that, except in the 10:1 RC mixture, most of these free RCs lacked a detectable His-tag, presumably due to its loss during purification, storage or due to photodamage during analysis under ambient illumination (Figure S8b, Supporting Information). The very small amount of intact His-tagged RCs in the free fraction underscored the tight binding interaction enabled by the tag. Therefore, to calculate $\tilde{v}$ for each mixture the concentration of free RCs in the mixture ([RC_{free}]) was adjusted for the concentration of RCs not bound to the QDs ([RC_{noHis}]) (see Equation 2 in Experimental Procedures).

The fit of the model summarised by Equation 2 to the average binding ratio $\tilde{v}$ obtained from the sucrose pull-down experiments is shown in Figure 7b. Parameters $\tilde{n}$ and k_{micro} from the fit were 15 and 8.23 μM^{-1}, respectively. The value of [RC_{noHis}] derived from the fit equated to 4.1 % of the total RC population. Conversion of the microscopic thermodynamic constant k_{micro} to macroscopic dissociation constants (K_d) at permitted valencies (i) using **Equation 3** in Experimental Procedures gave a high binding affinity with $K_{d,i=1}$ = 8.1 nM between a free QD and the first RC. Conjugate assembly and disassembly according to the model depicted in Figure 7a was addressed through the reaction scheme shown in **Equation 4** in Experimental Procedures, which produced

macroscopic kinetic constants for binding and dissociation at all permitted valencies (*i*). A deterministic model was then generated (**Equation 5.1-6.2**) that enabled an estimate of conjugate heterogeneity for any RC:QD ratio. Figure 7c shows the result for a 10:1 RC:QD mixture ([QD] = 50 nM), with a mean of 7.7 RCs per QD and individual stoichiometries ranging from 1:1 to 15:1. Simulation results and determined distributions of actual RC:QD stoichiometries for other overall ratios of RC:QD are summarized, respectively, in Figure S9 and Figure S10, Supporting information.

It was previously reported that the stoichiometry of conjugates formed between His-tagged maltose binding protein (MBP) and QDs follows a Poisson distribution[40]. Comparison of the present simulation result to a Poisson distribution with the same mean showed a broadly similar but not identical structure especially at high RC:QD ratios (Figure 7C). A more realistic explanation of the observed heterogeneity in RC:QD stoichiometry is that formation of RC_i/QD conjugates (where $i = 1,2,\ldots,\tilde{n}$) depends on all previous species, whereas a Poisson distribution assumes every event happens independently. This could explain why the Poisson distribution predicts a higher population of complexes with a very high RC:QD stoichiometry than the simulation.

2.7. Estimations of FRET efficiency and distance.

The standard analysis of a FRET interaction considers a donor-acceptor pair, but in the present case, even at RC:QD ratios below unity, an individual QD donor can accommodate multiple RC acceptors. Accordingly, the average energy transfer efficiency between a single QD-RC pair (E_{DA}) was calculated using **Equation 7 (**see Experimental Procedures), which took into account the heterogeneity in QD:RC stoichiometry. The theoretical correlation between E_{DA} and the apparent

efficiency for a multiple acceptor system (E_{app}) is shown in **Figure 8**a**.** The relationship was close to linear for conjugates where the average RC:QD was below one, and became increasingly non-linear as RC:QD increased. This non-linear relationship underscored the importance of accounting for heterogeneity in seeking a precise understanding of the efficiency of FRET from a QD to multiple bound RCs. Based on these above considerations, single QD-RC pair FRET efficiencies at different RC:QD ratios were estimated using Equation 7**.** Values increased as the RC:QD ratio increased and plateaued above a 5:1 ratio at a value of around 0.64 for conjugates formed from WT RCs (Figure 8b). Uniformly higher FRET efficiencies were obtained for the three BPhe replacement mutants for every assessed RC:QD ratio (Figure 8b), again maximising at a RC:QD of 5:1. This higher efficiency likely arises from the greater spectral overlap (see above)

The actual FRET distance (R) for different RC:QD ratios was evaluated from half efficiency distances calculated using **Equations 8** and **9** (see Experimental Procedures). This required determination of the QD quantum yield, as described in Experimental Procedures and summarised in Figure S11, Supporting Information. The values of R arrived at for the WT_H RC and cofactor replacement mutants were physically reasonable, for WT_H varying between ~7.0 nm for the lowest RC:QD ratio and dropping to ~6.4 nm for the highest RC:QD ratio (Figure 8c). The calculated conjugate diameter based on the FRET distances was 22.1 ± 0.2 nm and 20.9 ± 0.1 nm from the lowest and highest RC:QD ratios (assuming the FRET distance is from the center of the QD to the center of the four acceptor RC bacteriochlorins). These deduced conjugate diameters were very close to the value of 21.4 nm estimated from TEM. Consistency in the calculated FRET distances for the WT_H RC and three BPhe replacement mutant RCs suggested the generally improved QD emission quenching seen with the latter is indeed due to their altered absorption spectra and improved spectral overlap with the QD emission.

3. Discussion

As outlined in the Introduction, there is growing interest in the use of proteins from the photosystems of *Rba. sphaeroides* and related anoxygenic purple photosynthetic bacteria in devices that take advantage of their highly quantum-efficient light harvesting and separation of electrical charge.[8,11,12] A drawback, however, is their limited energy harvesting across a large part of the visible region of the solar spectrum.

One option to address this is to artificially augment the light harvesting capacity of the *Rba. sphaeroides* RC.[49] Published approaches include the direct attachment of blue-absorbing or green/red-absorbing synthetic dyes to lysine residues on a carotenoid-less RC,[50,51] the direct attachment of green/red or red/nearIR-absorbing dyes to cysteine residues engineered on native RCs[52] and the attachment of pairs of dyes carried on a DNA nanoscaffold.[53] These provide a means of adding multiple chromophores to a RC, although it is difficult to control their spatial arrangement when multiple attachment sites are present. Augmented energy harvesting has also been studied in a fusion protein between a carotenoid-deficient RC and a yellow fluorescent protein.[54]

Three previous experimental studies have looked at energy transfer between purified *Rba. sphaeroides* RCs and water-soluble QDs,[55–57] All three of these somewhat related studies employed WT RCs without a His-tag that had been purified from a native strain of *Rba. sphaeroides* through LDAO-solubilisation and hydroxyapatite column chromatography. Where discussed, the binding of RCs to QDs inferred from quenching of QD emission was attributed to unspecified electrostatic interactions. In contrast, in the present work a His-tag was used to bind RCs to QDs with nanomolar affinity for the first interaction and in an oriented fashion with the

bacteriochlorin cofactors closest to the QD. This tight and specific binding allowed conjugate formation at a QD concentration of 50 nM, some 5-20 fold lower than in previous work[55–57], avoiding the need to correct data for inner filter and reabsorption effects arising from micromolar concentrations of RC ([RC] was maximally 500 nM in the present work). His-tagged RCs were also purified from strains of *Rba. sphaeroides* lacking the genes that encode the light harvesting complexes [58], precluding contamination of RCs with LH2 complexes as reported previously [55]. We have also employed site-directed mutagenesis to remove the RC carotenoid to enable more selective QD excitation, to vary donor-acceptor spectral overlap by replacing BPhe cofactors with BChls, and to render the RC fluorescent to confirm the energetic link between RCs and QDs.

The His-tag used to anchor the RC to the surface of a QD was genetically engineered to the protein by a linker sequence that can be modified at will. As the dimensions of the QDs and RCs are known, and the maximum length of the linker can be estimated, it is possible to deduce the number of RCs that can pack around a QD at different RC-QD separations dictated by the linker length. This was done by reducing the problem to the number of circles of a diameter of 10 nm, representing the maximum cross-section of a RC-detergent micelle complex, that can fit on a spherical surface of different diameters (Figure S12, Supporting Information). The permitted number of RC-detergent complexes is 4 at a separation (i.e. linker length) of 0 nm and increases to 17 at a maximal separation of 6.08 nm (Table S1, Supporting Information). This upper packing limit corresponded reasonably well to an upper limit of 15 RCs per QD derived from modelling of the RC-QD interaction (see Figure 7; Figure S12, Supporting Information).

A notable variance from previously published work was the high ratio of RC:QD (10:1) required for quenching of QD emission (~92 %) in the present study. In the most comparable previous example, Maksimov and co-workers[57] reported a maximum of 85% quenching of 780

nm emission from CdTe QDs at a RC:QD of 3.6. This much lower maximal ratio with similarly sized QDs is consistent with direct electrostatic binding of RCs to the 780 nm QDs that saturates around a ratio of 4 RCs per QD (Table S1, Supporting Information). Previous titrations of smaller QDs with RCs have also reported maximum quenching as occurring at ratios of between 2 and 6 RCs per QD, consistent with direct electrostatic binding of the protein to the QD surface that limits the number of RCs that can pack around a QD. A drawback is that this type of binding interaction cannot be easily manipulated. In contrast, the strategy of using a His-tag and linker in the present work not only facilitated strong and specific binding but also permitted a larger number of RCs to be assembled around each QD due to the details of a programmable linker, maximising the extent of QD emission quenching.

The principal conclusion arrived at in this study is that energy is passed from QDs to bound RCs by FRET, with no indication of energy transfer mediated by an alternative process such as electron exchange. Measurements revealing QD enhancement of RC photobleaching in WT_H and carotenoid-less RCs, and enhancement of BChl emission from P-less RCs, clearly showed that energy is passed from QDs to the RC BPhe and monomeric BChl pigments when a conjugate is formed between multiple proteins and a QD. Quenching was not seen using other His-tagged proteins, or following SDS/heat treatment to unfold intact WT_H RCs, or following imidazole/histidine treatment to unbind WT_H RCs, or following protease treatment to detach the WT_H RC from its tag, showing it to be dependent on conjugation to structurally-intact RCs. In contrast, quenching was unaffected by removal of the carotenoid cofactor, replacement of one or both of the RC BPhes with BChl, or removal of the primary donor BChls, showing that it did not involve the carotenoid cofactor or require the operation of conventional photochemical charge separation. We conclude from this that the basic requirement for quenching of QD emission by

RCs is one or more BChl or BPhe pigments with absorbance that overlaps with the QD emission band. Once transferred, energy can be dissipated through charge separation (as in the WT_H and cofactor replacement mutants) or BChl or BPhe emission (as in the $VL157R_H$ P-less RC).

An interesting observation made with $VL157R_H$/QD conjugates was that RC emission initially increased as the RC:QD ratio increased up to a value of 2.5:1, as might be expected given the associated increase in quenching of QD emission, but then declined as this ratio increased further to 5:1 and then 10:1 despite the fact that quenching of QD emission continued to increase. The reason for this remains to be confirmed but the most likely is exciton-exciton annihilation. Such annihilation processes are well documented in natural arrays of purple bacterial light harvesting complexes,[59,60] and in recent years have been studied systematically in LH2 arrays reconstituted into artificial bilayers,[61,62] but would not normally be detected in purple bacterial RCs due to efficient energy trapping by charge separation.

Heterogeneity in the number of RCs per QD is a factor that has an influence over the analysis of the efficiency of FRET. In the present work this heterogeneity could be well-explained by thermodynamic scheme based on an independent binding model. Although the QD surface did not offer a distinct number of discrete "binding sites", the model offered a good approximation of the conjugation process between multiple RCs and a QD. Considering that protein/QD conjugation is the result of a collision between the protein His-tag and the QD surface, when any "binding site" is already occupied by a protein, further attachments to this area are prohibited. Also, because of the dynamics of a protein attached to a site by a flexible linker, the shielding of binding could happen over a rather larger area than that of the protein itself and might be affected by neighbouring proteins. In addition, there is potential for reorganisation of bound proteins on the QD surface. Taking these factors together, it is to be expected that the final number of "binding

sites" will be heterogeneous around an average. It has been reported that the kinetics of His-tag mediated binding of proteins to QDs occurs rapidly[63] and we also observed that self-assembly was stable within a few minutes of initiation of binding, indicating that the system was at equilibrium (e.g. see Figure S1b; Figure S9, Supporting Information). Using fitted parameters, the fractions of self-assembled conjugates with a certain number of RCs per QD could be assigned, producing a profile that closely matched a Poisson distribution (Figure 7c). The model also enabled effects stemming from variation of sample concentration to be accounted for. In addition, the model provided a kinetic understanding of why protein-QD conjugation approximated to Poisson statistics and revealed that the variance between the simulation and Poisson statistics could be the consequence of a dependence of the number proteins per QD on previous species. The knowledge generated on RC-QD conjugation could be readily transferred to other protein/nanomaterial self-assembling systems and, moreover, opens the possibility of decoding heterogeneity in conjugated systems that are more complex than just one protein and one nanoparticle.

FRET distances and efficiencies were estimated through a process that took into account RC:QD heterogeneity (Figure 8). The FRET efficiencies of the WT_H RC and all BPhe-replacement mutants increased with an increasing RC:QD ratio, with high ratio RC/QD conjugates showing an apparent ~0.6 nm decrease in FRET distance relative to low ratio conjugates (Figure 8c). FRET efficiency was also higher in the high ratio conjugates than in the low ratio conjugates (Figure 8b). Intriguingly, a transition was observed in both parameters around a RC:QD of 2.5, with less variation before/after this region. A RC:QD ratio of 2.5 also marked the point at which emission from P-deficient $VL157R_H$ RCs was maximal, and we suggest that these trends are manifestations of the influence of increasing crowdedness in the shell of bound proteins. In the case of $VL157R_H$ RCs, emission increases up to a RC:QD of 2.5 as more energy is passed from the QD to the

surrounding RCs. Beyond this point increased protein crowding causes the mean inter-protein distance to fall below the exciton diffusion radius and multiple excited states could co-exist in a single conjugate with multiple RCs, allowing annihilation to occur and causing the amount of emission to progressively drop. One possibility is that the effect of crowding on FRET efficiency and distance could be attributable to the orientation factor, κ^2, that used to describe dipole-dipole coupling between donor and acceptor. For the purposes of calculating E_{DA} and R a value of ⅔ was assigned to κ^2, but it may be that this (commonly applied) simplification becomes less valid when the distribution of possible orientations between the QD and the four acceptor bacteriochlorins in each RC becomes more constrained in progressively more densely-packed RC/QD conjugates at the higher RC:QD ratios.

4. Conclusion

This report establishes that water-soluble CdTe QDs form a specific binding interaction with *Rba. sphaeroides* RCs when the latter are modified by an extra-membrane poly-histidine tag, the tag also serving to orient RCs at the QD surface. The dissociation constant between a single RC and QD was estimated as being 8.1 nM, indicating a tight binding interaction, and this interaction was well explained by a model assuming multiple, independent binding events. Monodispersed conjugates were directly visualized by negative stain TEM and were found to have a mean diameter of ~ 21.4 ± 1.0 nm. Bound RCs quenched QD fluorescence and, conversely, QD excitation drove photochemistry in WT or carotenoid-less RCs, and drove RC emission in photochemically-inactive RCs lacking the primary electron donor BChls. Quenching of QD emission was sensitive to the spectral overlap with RC absorbance, consistent with a FRET mechanism for the energy transfer. The estimated FRET distance R was consistent with

morphologies of the RC-QD conjugates predicted from modelling of the RC/QD interaction and measured through experiment. The single donor/acceptor FRET efficiency, E_{DA}, was of the order of 0.53 for the smallest conjugates involving WT_H RCs, and somewhat higher (0.55-0.6) for pigment-replacement mutant RCs with enhanced spectral overlap. A decrease in *R* and increase in E_{DA} was seen in larger RC/QD conjugates, effects we attribute to increased packing of RCs around a central QD that constrains their dynamic freedom. Evidence suggestive of exciton-exciton annihilation was also seen when photochemically-inactive RCs were packed around a central QD at a high RC:QD ratio. We conclude that stable conjugates of a well-defined composition can be formed between His-tagged RCs and water-soluble RCs. In addition to the QDs acting as a synthetic antenna to drive RC photochemistry, they also have potential to act as a hub for the assembly of more complex photosystems involving novel combinations of natural and synthetic components.

5. Experimental Procedure

5.1. RC expression and purification.

Wild-type (WT) and engineered RCs modified with a deca-histidine tag on the C-terminus of the M-polypeptide (denoted with subscript "H") were expressed in a strain of *Rba. sphaeroides* lacking light harvesting complexes.[58] Strain construction, cell growth and RC purification were carried out as described in detail previously,[64] with the exception that RCs purified by nickel affinity chromatography using lauryldimethylamine oxide (LDAO) as the solubilising detergent were exchanged into 20 mM Tris (pH 8)/0.04 % *N*-dodecyl β-D-maltoside (DDM) during gel filtration on a Superdex 200 column, and concentrated and stored in this buffer (referred to henceforth as Tris/DDM). Construction of RCs with the mutations GM71L, LL185H, LM214H

and LL185H/LM214H was as described previously,[44,46,47] with the exception that a deca-histidine tag was included as described above. In addition, a RC with the mutation valine 157 of the L-polypeptide to arginine (VL157R) was constructed.[45] The concentrations of the WT_H and $GM71L_H$ RCs were calculated using an extinction coefficient for the $B_{A/B}$ Q_y band at 804 nm of 288,000 $M^{-1}cm^{-1}$.[65] For the $LL185H_H$, $LM214H_H$ and $LL185H/LM214H_H$ RCs, extinction coefficients for the modified $B_{A/B}$ Q_y band were estimated by normalisation to the unmodified primary donor BChl Q_y absorption band at ~865 nm in spectra of the mutant and WT RCs recorded in the presence of 5 mM sodium ascorbate. An extinction coefficient for the modified $B_{A/B}$ Q_y band of the $VL157R_H$ RC was estimated by normalisation of its spectrum to that of the WT_H RC at the maximum of the unmodified $H_{A/B}$ Q_y band at ~760 nm.

5.2. XylE and eGFP expression and purification.

The gene for the *Escherichia* (*E.*) *coli* proton-coupled xylose transporter XylE was cloned into a pET28 vector and expressed in *E. coli* strain C43 (DE3). Expression was induced in 1 L cultures at a cell density of OD_{600} = 0.8 by adding 1 mM IPTG for 3 hours during growth in an orbital incubator at 250 rpm and 37°C. Harvested cell pellets were resuspended in 25 mM Tris-HCl (pH 8)/150 mM NaCl and a cOmplete™ EDTA-free protease inhibitor tablet and a few crystals of lyophilised DNase (Sigma Aldrich®) were added. Cells were lysed by two passes through a Constant Systems cell disrupter at 25 kPSI. Cell debris was removed by centrifugation 15,000 rpm for 15 mins at 4°C in an SS-34 rotor (Sorvall) and the membrane fraction isolated by centrifugation of the supernatant at 38,000 rpm for 1 hour at 4°C in a Ti45 rotor (Beckman). The resulting membrane pellet was resuspended in 25 mM Tris-HCl (pH 8)/150 mM NaCl and DDM was added to a final concentration of 1.5 % (w/v). After stirring for 1 h at 4°C membrane debris was removed

by centrifugation at 38,000 rpm for 1 hour at 4°C. The supernatant was diluted in 25 mM Tris-HCl (pH 8)/150 mM NaCl to achieve a final concentration of 1 % DDM and passed through a Ni-NTA column (5 mL; Qiagen™). Bound $XylE_H$ was eluted using 25 mM Tris-HCl (pH 8)/150 mM NaCl/300 mM imidazole/0.05 % DDM. The eluate was concentrated and the $XylE_H$ was further purified by gel-filtration chromatography using a Superdex 200 column equilibrated in 25 mM Tris-HCl (pH 8)/150 mM NaCl/0.05 % DDM. The $XylE_H$ peak was collected, concentrated, aliquoted, snap-frozen in liquid nitrogen and stored at -80°C. The concentration of $XylE_H$ was evaluated using *DC*™ protein assay (Bio-Rad).

A gene for His-tagged enhanced green fluorescent protein ($eGFP_H$) was cloned into pET28a and expressed in *E. coli* strain Rosetta™ 2 (DE3). Induction of expression, cell harvesting, cell lysis and removal of cell debris was as for purification of $XylE_H$. The supernatant from the clearing spin was passed through a HisTrap HP nickel affinity column and, after rinsing with 5 column volumes of 20 mM Tris (pH 8.0)/ 200 mM NaCl, bound $eGFP_H$ was eluted in the same buffer supplemented with 500 mM imidazole. $eGFP_H$ fractions were pooled and concentrated, and further purification achieved by gel-filtration chromatography using a Superdex 200 column equilibrated in 20 mM Tris (pH 8.0). The $eGFP_H$ peak was collected, concentrated, aliquoted, snap-frozen in liquid nitrogen and stored at -80°C.

5.3. QD and RC titrations.

Water-soluble Cd/Te QDs coated with 3-mercaptopropionic acid with an emission maximum at 750 ± 5 nm were purchased from PlasmaChem GmbH. The supplied average molecular weight of these QDs (550 KDa) was used to calculate their molar concentration. QD emission was measured on a Cary Eclipse Fluorescence Spectrometer (Agilent™) with a microplate attachment,

using black 96-well microplates (Greiner Bio-One™) and a standard sample volume (100 µL). The spectrophotometer light source was a pulsed xenon lamp operating at 80 Hz and with a pulse full width at half maximum (FWHM) of 2 µs.

Titrations of QD emission were carried out using 50 nM QD in Tris/DDM, with varying concentrations of RC or other proteins. QD emission spectra were baseline corrected if required. For titrations with fluorescent VL157R_H RCs, baseline corrected spectra were deconvoluted to distinguish emission from the QDs at 750 nm and the RC at 800 nm. All titrations were carried out in triplicate unless stated otherwise.

5.4. Isolation of RC:QD conjugates on sucrose density gradients.

RC:QD conjugates were separated from free RCs on two step discontinuous sucrose density gradients formed from equal volumes of 25 % and 60 % (w/v) sucrose in Tris/DDM in ultraclear™ ultracentrifuge tubes (12 mL). A standard loading of a 2.5 µM RC solution (400 µL) was used with a varying concentration of QDs; samples were then overlaid with Tris/DDM (1 mL) to form a second step. Gradients were centrifuged at 38,000 rpm at 19^{o}C for 4 hours using a TH-641 swing-out rotor (Sorvall™) and deconstructed in ten 1 mL fractions and one 1.4 mL fraction by puncturing the bottom of the tube and collecting the contents dropwise. Fractions 9-11 from the top of the gradient corresponded to free RCs. Fractions 1-8 from the bottom and middle of the gradient corresponded to RC/QD conjugates and a small population of RCs released from QDs during the fractionation run.

Fractions from the 0 %/25 % interface containing free RCs were analysed by Tris-Glycine SDS-PAGE. Loaded 4%-20% Mini-PROTEAN® TGX™ Precast Protein Gels were run at 200 V for 45 mins and stained using Sypro® Ruby (Invitrogen™). Washed gels were visualized using a

Gel Doc™ EZ System (Bio-Rad). For Western blots, protein transfer was achieved using a TE 77 PWR Semi Dry Transfer Unit (GE Healthcare) at 45 mA/gel for an hour with 20 % methanol (v/v), 39 mM glycine, 48 mM Tris (pH 9.2) as transfer buffer. After overnight blocking of the membrane with 5 % (w/v) milk powder in phosphate buffered saline (PBS)/0.01 % Tween-20 (PBS/Tween), the membrane was incubated with monoclonal anti-polyhistidine peroxidase antibody (Sigma-Aldrich®) in 5 % milk/PBS/Tween for 1 h and then washed three times with PBS/Tween. Anti-His signals were developed using 1 x LumiGLO® (Cell Signalling Technology) for no more than 1 min. Developed membranes were visualised using an ODYSSEY Imaging System (LI-COR Biosciences).

5.5. Dynamic light scattering.

Particle sizes were measured on a Zetasizer Nano ZSP (Malvern Instruments Ltd). Samples were pre-equilibrated at 25°C for 5 mins and data were collected at 173° forward scattering with five repeats. Average particle sizes were computed from the intensity distribution peaks.

5.6. Transmission electron microscopy.

Negative staining of protein:QD conjugates for TEM was carried out on conjugates formed from a 10:1 RC:QD mix at a QD concentration of 100 nM. A drop of sample was applied to a glow discharge treated carbon coated grid and incubated for 30 s. Excess sample was removed using filter paper, the grid was immediately floated on top of a 3 % uranyl acetate (Sigma) droplet and excess liquid again removed using filter paper. After repeating this once, the grid was placed onto a third droplet of uranyl acetate for 1 min.[66] The grid was then washed with a droplet of water and completely dried in air before imaging with a Tecnai 12 120kV BioTwin Spirit TEM.

TEM images were analysed in Matlab (MathWorks). Most identified particles were approximately spherical in shape (Figure S7b-c, Supporting Information), distinct from isolated QDs (Figure S7a, Supporting Information) and their diameters were in the physically permitted range. A final manual check was carried out to exclude any objects with a false outline, and particle diameters were fitted to a lognormal distribution.

5.7. Determination of QD quantum yield.

The quantum yield of the water-soluble QDs (Φ_{QD}) in Tris/DDM was determined by comparison to the dye LDS-751 (Sigma) dissolved in methanol[67] with a Varian Cary Eclipse Fluorimeter. Potential effects of protein attachment were accounted for by incubating QDs with the His-tagged, DDM-solubilised photochemically-inactive membrane protein $XylE_H$ at the same ratios as used for RC_H/QD measurements. To avoid self-shading the absorbance of $XylE_H$/QD conjugates and LDS-751 was limited to 0.025 at the 550 nm excitation wavelength (Figure S11a, Supporting Information). Emission from LDS-751 and QDs or $XylE_H$/QD conjugates after 550 nm excitation (average of 10 measurements; Figure S11b, Supporting Information) was corrected with spectral response and used to calculate the relative integral photon fluxes of QDs and LDS-751.[68] The value for Φ_{QD} was estimated with reference to $\Phi_{LDS\text{-}751} = 0.014$ and the value of refractive index of water ($n_{water} = 1.333$) and methanol ($n_{methanol} = 1.328$).[69] The estimated Φ_{QD} for $XylE_H$/QD conjugates was constant over the range of protein to QD ratios examined (Figure S11c, Supporting Information) and the average value of 0.197 was used for calculating FRET distance.

5.8. Photo-oxidation of the RC primary electron donor.

Measurements of photo-oxidation of the RC primary electron donor at 870 nm were carried out using a Cary60 absorbance spectrophotometer fitted with an optical fiber attachment and a four-way cuvette holder (Ocean Optics, Inc.). For preferential QD excitation, light from a HL-2000 tungsten halogen source (Ocean Optics, Inc.) was passed through an optical fiber and a 450 ± 25 nm band-pass filter (Edmund Optics Ltd). Illumination time was controlled using a TGP110 pulse generator (Aim-TTi Ltd, UK) to operate the electronic shutter on the light source. Samples of RC/QD conjugate (RC:QD = 2.5, [QD] = 2 μM) were housed in a 3 mm path length, four-sided micro cuvette (110-15-QS, Hellma® Analytics). Each measurement was repeated five times and averaged traces were fitted to a model assuming interconversion between the ground (P) and photo-oxidised state (P^+) of the RC primary donor:

$$P \underset{k_r}{\overset{k_f}{\leftrightarrows}} P^+ \qquad (1)$$

where k_f is positively correlated with the energy utilised by the RC.

The recovery of RC ground state absorbance after white light illumination for 0.5 s was also measured with the same setup minus the bandpass filter. Recovery rates were determined from traces that were the average of five repeats.

5.9. Simulation of RC/QD binding.

Average numbers of RCs bound to each QD at different RC:QD ratios, calculated from fractions 1-8 in sucrose gradient pulldown experiments (see above), were plotted against the concentration of free RCs [RC_{free}] calculated from fractions 9-11. Data in this plot were fitted with a model that considered that the association of each RC to a QD was an independent event and the QD provided multiple identical binding sites.[43] The concentration of free RCs in the model

([RC_{free}]) was adjusted for the experimental finding that most unbound RCs had lost their His-tag [RC_{noHis}]. The final model comprised:

$$\bar{v} = \frac{\tilde{n} k_{micro}([RC_{free}] - [RC_{noHis}])}{1 + k_{micro}([RC_{free}] - [RC_{noHis}])} \quad (2)$$

The terms deduced from the fit were the microscopic thermodynamic association constant (k_{micro}), the maximum number of RCs binding to each QD ($\tilde{n}$) and [RC_{noHis}]. Parameters k_{micro} and $\tilde{n}$ were then used to determine macroscopic dissociation constants (K_d) at permitted valencies (i) from

$$K_{d,i} = \frac{i}{(\tilde{n} - 1 + i)k_{micro}} \quad (i = 1, 2, ..., \tilde{n}) \quad (3)$$

Conjugate assembly and disassembly was addressed through the model depicted in Figure 7a and the reaction scheme:

$$RC_{His} + RC_{i-1}QD \underset{k_{r,i}}{\overset{k_{f,i}}{\rightleftharpoons}} RC_iQD \quad (i = 1, 2, ..., \tilde{n}) \quad (4)$$

where RC_{His} is the total RC population adjusted for RCs without a His-tag and so unable to bind, and $k_{f,i}$ and $k_{r,i}$ are the macroscopic kinetic constants for binding and dissociation, respectively, at permitted valencies (i) from 0 to $\tilde{n}$.

A set of ordinary differentiation equations (ODEs) was then generated:

$$\frac{d[RC_{His}]}{dt} = -[RC_{His}]\sum_{i=1}^{\tilde{n}}(k_{f,i}[RC_{i-1}QD] + k_{r,i}[RC_iQD]) \quad (5.1)$$

$$\begin{aligned}\frac{d[RC_iQD]}{dt} =& [RC_{His}](k_{f,i}[RC_{i-1}QD] - k_{f,i+1}[RC_iQD]) \\ &+ k_{r,i+1}[RC_{i+1}QD] - k_{r,i}[RC_iQD] \quad (i = 0, 1, 2, ..., \tilde{n})\end{aligned} \quad (5.2)$$

where $k_{f,i}[RC_{i-1}QD]$ at $i = 0$ and $k_{r,i+1}[RC_{i+1}QD]$ at $i = \tilde{n}$ were omitted. The macroscopic kinetic constants $k_{f,i}$ and $k_{r,i}$ used in Equations 5.1,5.2 were determined from their corresponding microscopic kinetic constants using:

$$k_{f,i} = (\tilde{n} + 1 - i)k_{on,micro} \quad (i = 0, 1, 2, ..., \tilde{n}) \quad (6.1)$$

$$k_{r,i} = ik_{off,micro} \quad (i = 0, 1, 2, ..., \tilde{n}) \quad (6.2)$$

A deterministic simulation was carried out in MATLAB using the ODEs and the defined kinetic constants. Distributions of the binding stoichiometry were deduced after the model relaxed to equilibrium and were compared with a Poisson distribution at the same mean.

5.10. Estimation of FRET efficiency and distance.

Apparent FRET efficiencies, E_{app}, obtained from titrations of QD fluorescence by WT_H RCs were used to determine the average FRET efficiency of single RC-QD pair, E_{DA}, from:

$$E_{app} = \sum_{i=1}^{\tilde{n}} p(i)\frac{iE_{DA}(i)}{(i-1)E_{DA} + 1} \quad (7)$$

The term $p(i)$ where (i = 1,2,…,$\tilde{n}$) represented the distribution of conjugates with different numbers of RC_H per QD. Values of p were determined from the simulation described above.

The distance for 50 % FRET efficiency, R_0, was determined from[39]:

$$R_o^6 = 8.785 \times 10^{-25} \frac{\Phi_D \kappa^2 J}{n^4} \quad (in\ cm^6) \qquad (8)$$

where Φ_D is the QD quantum yield, J is the spectral overlap between donor fluorescence and acceptor absorbance, and n is the refractive index of water (1.33). The orientation factor κ^2 was assumed to be ⅔.

Having determined E_{DA} and R_0, the actual FRET distance, R, was then estimated using:

$$E_{DA} = \frac{R_o^6}{R_o^6 + R^6} \qquad (9)$$

Supporting Information

Supporting Information is available from the Wiley Online Library or from the author.

Acknowledgements

JL and MRJ acknowledge funding from the EPSRC/BBSRC Synthetic Biology Centre for Doctoral Training (EP/L016494/1) and from the BrisSynBio Synthetic Biology Research Centre at the University of Bristol (BB/L01386X/1). The authors wish to thank University of Bristol students Benjamin M. Vos, Michael C. James, Frank Rui and Alexander Van De Steen for contributions to preliminary experiments.

Received: ((will be filled in by the editorial staff))

Revised: ((will be filled in by the editorial staff))

Published online: ((will be filled in by the editorial staff))

References

[1] G. Renger, *Curr. Sci.* **2010**, *98*, 1305.

[2] P. Heathcote, M. R. Jones, in *Compr. Biophys.* (Eds: E.H. Egelman, S. Ferguson), Academic Press, Oxford, UK, **2012**, pp. 115–144.

[3] N. Nelson, W. Junge, *Annu. Rev. Biochem.* **2015**, *84*, 659.

[4] S. Duan, C. Dall'Agnese, G. Chen, X. F. Wang, H. Tamiaki, Y. Yamamoto, T. Ikeuchi, S. I. Sasaki, *ACS Energy Lett.* **2018**, *3*, 1708.

[5] A. Badura, T. Kothe, W. Schuhmann, M. Rögner, *Energy Environ. Sci.* **2011**, *4*, 3263.

[6] A. A. Boghossian, M.-H. Ham, J. H. Choi, M. S. Strano, *Energy Environ. Sci.* **2011**, *4*, 3834.

[7] F. Wang, X. Liu, I. Willner, *Adv. Mater.* **2013**, *25*, 349.

[8] Y. Kim, S. A. Shin, J. Lee, K. D. Yang, K. T. Nam, *Nanotechnology* **2014**, *25*, 1.

[9] K. Nguyen, B. D. Bruce, *Biochim. Biophys. Acta - Bioenerg.* **2014**, *1837*, 1553.

[10] O. Yehezkeli, R. Tel-Vered, D. Michaeli, I. Willner, R. Nechushtai, *Photosynth. Res.* **2014**, *120*, 71.

[11] S. K. Ravi, S. C. Tan, *Energy Environ. Sci.* **2015**, *8*, 2551.

[12] V. M. Friebe, R. N. Frese, *Curr. Opin. Electrochem.* **2017**, *5*, 126.

[13] S. K. Ravi, V. S. Udayagiri, L. Suresh, S. C. Tan, *Adv. Funct. Mater.* **2017**, *28*, 1.

[14] M. Chatzipetrou, F. Milano, L. Giotta, D. Chirizzi, M. Trotta, M. Massaouti, M. R. Guascito, I. Zergioti, *Electrochem. Commun.* **2016**, *64*, 46.

[15] T. Szabó, R. Csekő, K. Hajdu, K. Nagy, O. Sipos, P. Galajda, G. Garab, L. Nagy, *Photosynth. Res.* **2017**, *132*, 127.

[16] N. Terasaki, N. Yamamoto, K. Tamada, M. Hattori, T. Hiraga, A. Tohri, I. Sato, M. Iwai, M. Iwai, S. Taguchi, I. Enami, Y. Inoue, Y. Yamanoi, T. Yonezawa, K. Mizuno, M. Murata, H. Nishihara, S. Yoneyama, M. Minakata, T. Ohmori, M. Sakai, M. Fujii, *Biochim. Biophys. Acta - Bioenerg.* **2007**, *1767*, 653.

[17] H. Krassen, A. Schwarze, B. Friedrich, K. Ataka, O. Lenz, J. Heberle, *ACS Nano* **2009**, *3*, 4055.

[18] J. W. K. Oliver, S. Atsumi, *Photosynth. Res.* **2014**, *120*, 249.

[19] A. Efrati, C.-H. Lu, D. Michaeli, R. Nechushtai, S. Alsaoub, W. Schuhmann, I. Willner, *Nat. Energy* **2016**, *1*, 15021.

[20] P. Jordan, P. Fromme, H. T. Witt, O. Klukas, W. Saenger, N. Krauß, *Nature* **2001**, *411*, 909.

[21] I. Grotjohann, P. Fromme, *Photosynth. Res.* **2005**, *85*, 51.

[22] J. Kargul, J. D. Janna Olmos, T. Krupnik, *J. Plant Physiol.* **2012**, *169*, 1639.

[23] G. Feher, J. P. Allen, M. Y. Okamura, D. C. Rees, *Nature* **1989**, *339*, 111.

[24] A. J. Hoff, J. Deisenhofer, *Phys. Rep.* **1997**, *287*, 1.

[25] W. Zinth, J. Wachtveitl, *ChemPhysChem* **2005**, *6*, 871.

[26] M. R. Jones, *Biochem. Soc. Trans.* **2009**, *37*, 400.

[27] R. E. Blankenship, D. M. Tiede, J. Barber, G. W. Brudvig, G. Fleming, M. Ghirardi, M. R. Gunner, W. Junge, D. M. Kramer, A. Melis, T. A. Moore, C. C. Moser, D. G. Nocera, A. J. Nozik, D. R. Ort, W. W. Parson, R. C. Prince, R. T. Sayre, *Science* **2011**, *332*, 805.

[28] S. C. Tan, L. I. Crouch, M. R. Jones, M. Welland, *Angew. Chemie - Int. Ed.* **2012**, *51*, 6667.

[29] S. M. Mirvakili, J. E. Slota, A. R. Usgaocar, A. Mahmoudzadeh, D. Jun, M. N. Mirvakili, J. T. Beatty, J. D. W. Madden, *Adv. Funct. Mater.* **2014**, *24*, 4789.

[30] H. Yaghoubi, E. Lafalce, D. Jun, X. Jiang, J. T. Beatty, A. Takshi, *Biomacromolecules* **2015**, *16*, 1112.

[31] V. M. Friebe, J. D. Delgado, D. J. K. Swainsbury, J. M. Gruber, A. Chanaewa, R. Van Grondelle, E. Von Hauff, D. Millo, M. R. Jones, R. N. Frese, *Adv. Funct. Mater.* **2016**, *26*, 285.

[32] S. K. Ravi, Z. Yu, D. J. K. Swainsbury, J. Ouyang, M. R. Jones, S. C. Tan, *Adv. Energy Mater.* **2017**, *7*, 1.

[33] S. K. Ravi, D. J. K. Swainsbury, V. K. Singh, Y. K. Ngeow, M. R. Jones, S. C. Tan, *Adv.*

Mater. **2018**, *30*, 1.

[34] I. L. Medintz, H. Mattoussi, *Phys. Chem. Chem. Phys.* **2009**, *11*, 17.

[35] H. K. Jun, M. A. Careem, A. K. Arof, *Renew. Sustain. Energy Rev.* **2013**, *22*, 148.

[36] M. A. Walling, J. A. Novak, J. R. E. Shepard, *Int. J. Mol. Sci.* **2009**, *10*, 441.

[37] M. H. Vos, J. Breton, J.-L. Martin, *J. Phys. Chem. B* **1997**, *101*, 9820.

[38] X. J. Jordanides, G. D. Scholes, G. R. Fleming, *J. Phys. Chem. B* **2001**, *105*, 1652.

[39] R. M. Clegg, *Methods Enzymol.* **1992**, *211*, 353.

[40] T. Pons, I. I. L. Medintz, X. Wang, D. S. English, H. Mattoussi, *J. Am. Chem. Soc.* **2006**, *128*, 15324.

[41] X. Ji, W. Wang, H. Mattoussi, *Nano Today* **2015**, *11*, 98.

[42] A. O. Govorov, *Adv. Mater.* **2008**, *20*, 4330.

[43] J. C. Martinez, J. Murciano-Calles, E. S. Cobos, M. Iglesias-Bexiga, I. Luque, J. Ruiz-Sanz, J. Murciano Calles, E. S. Cobos, M. Iglesias Bexiga, I. Luque, J. Ruiz Sanz, in *Appl. Calorim. a Wide Context* (Eds: E.S. Cobos, A.A. Elkordy), InTech, **2013**, pp. 73–104.

[44] J. P. Ridge, M. E. Van Brederode, M. G. Goodwin, R. Van Grondelle, M. R. Jones, *Photosynth. Res.* **1999**, *59*, 9.

[45] J. A. Jackson, S. Lin, A. K. W. Taguchi, J. C. Williams, J. P. Allen, N. W. Woodbury, *J. Phys. Chem. B* **1997**, *101*, 5747.

[46] C. Kirmaier, D. Gaul, R. DeBey, D. Holten, C. Schenck, *Science* **1991**, *251*, 922.

[47] A. J. Watson, P. K. Fyfe, D. Frolov, M. C. Wakeham, E. Nabedryk, R. Van Grondelle, J. Breton, M. R. Jones, *Biochim. Biophys. Acta - Bioenerg.* **2005**, *1710*, 34.

[48] W. G. Miller, C. V. Goebel, *Biochemistry* **1968**, *7*, 3925.

[49] A. Operamolla, R. Ragni, F. Milano, R. R. Tangorra, A. Antonucci, A. Agostiano, M.

Trotta, G. Farinola, *J. Mater. Chem. C* **2015**, *3*, 6471.

[50] F. Milano, R. R. Tangorra, O. Hassan Omar, R. Ragni, A. Operamolla, A. Agostiano, G. M. Farinola, M. Trotta, *Angew. Chemie - Int. Ed.* **2012**, *51*, 11019.

[51] O. Hassan Omar, S. La Gatta, R. R. Tangorra, F. Milano, R. Ragni, A. Operamolla, R. Argazzi, C. Chiorboli, A. Agostiano, M. Trotta, G. M. Farinola, *Bioconjug. Chem.* **2016**, *27*, 1614.

[52] P. K. Dutta, S. Lin, A. Loskutov, S. Levenberg, D. Jun, R. Saer, J. T. Beatty, Y. Liu, H. Yan, N. W. Woodbury, *J. Am. Chem. Soc.* **2014**, *136*, 4599.

[53] P. K. Dutta, S. Levenberg, A. Loskutov, D. Jun, R. Saer, J. T. Beatty, S. Lin, Y. Liu, N. W. Woodbury, H. Yan, *J. Am. Chem. Soc.* **2014**, *136*, 16618.

[54] K. J. Grayson, K. M. Faries, X. Huang, P. Qian, P. Dilbeck, E. C. Martin, A. Hitchcock, C. Vasilev, J. M. Yuen, D. M. Niedzwiedzki, G. J. Leggett, D. Holten, C. Kirmaier, C. N. Hunter, *Nat. Commun.* **2017**, *8*, 1.

[55] I. Nabiev, A. Rakovich, A. Sukhanova, E. Lukashev, V. Zagidullin, V. Pachenko, Y. P. Rakovich, J. F. Donegan, A. B. Rubin, A. O. Govorov, *Angew. Chemie - Int. Ed.* **2010**, *49*, 7217.

[56] E. P. Lukashev, P. P. Knox, I. P. Oleinikov, N. K. Seifullina, N. P. Grishanova, *Biochemistry* **2016**, *81*, 58.

[57] E. G. Maksimov, E. P. Lukashev, N. K. Seifullina, G. V. Nizova, V. Z. Pashchenko, *Nanotechnol. Russ.* **2013**, *8*, 423.

[58] M. R. Jones, G. J. S. Fowler, L. C. D. Gibson, G. G. Grief, J. D. Olsen, W. Crielaard, C. N. Hunter, *Mol. Microbiol.* **1992**, *6*, 1173.

[59] A. J. Campillo, R. C. Hyer, T. G. Monger, W. W. Parson, S. L. Shapiro, *Proc. Natl. Acad.*

Sci. U. S. A. **1977**, *74*, 1997.

[60] L. Valkunas, G. Trinkunas, V. Liuolia, R. van Grondelle, *Biophys. J.* **1995**, *69*, 1117.

[61] T. J. Pflock, S. Oellerich, L. Krapf, J. Southall, R. J. Cogdell, G. M. Ullmann, J. Köhler, *J. Phys. Chem. B* **2011**, *115*, 8821.

[62] A. Sumino, T. Dewa, T. Noji, Y. Nakano, N. Watanabe, R. Hildner, N. Bösch, J. Köhler, M. Nango, *J. Phys. Chem. B* **2013**, *117*, 10395.

[63] K. E. Sapsford, T. Pons, I. L. Medintz, S. Higashiya, F. M. Brunel, P. E. Dawson, H. Mattoussi, *J. Phys. Chem. C* **2007**, *111*, 11528.

[64] D. J. K. Swainsbury, V. M. Friebe, R. N. Frese, M. R. Jones, *Biosens. Bioelectron.* **2014**, *58*, 172.

[65] S. C. Straley, W. W. Parson, D. C. Mauzerall, R. K. Clayton, *BBA - Bioenerg.* **1973**, *305*, 597.

[66] M. Rames, Y. Yu, G. Ren, *J. Vis. Exp.* **2014**, *15*, 1.

[67] C. Würth, M. Grabolle, J. Pauli, M. Spieles, U. Resch-Genger, *Nat. Protoc.* **2013**, *8*, 1535.

[68] J. A. Gardecki, M. Maroncelli, *Appl. Spectrosc.* **1998**, *52*, 1179.

[69] P.-C. Wu, C.-Y. Chen, C.-W. Chang, *New J. Chem.* **2018**, *42*, 3459.

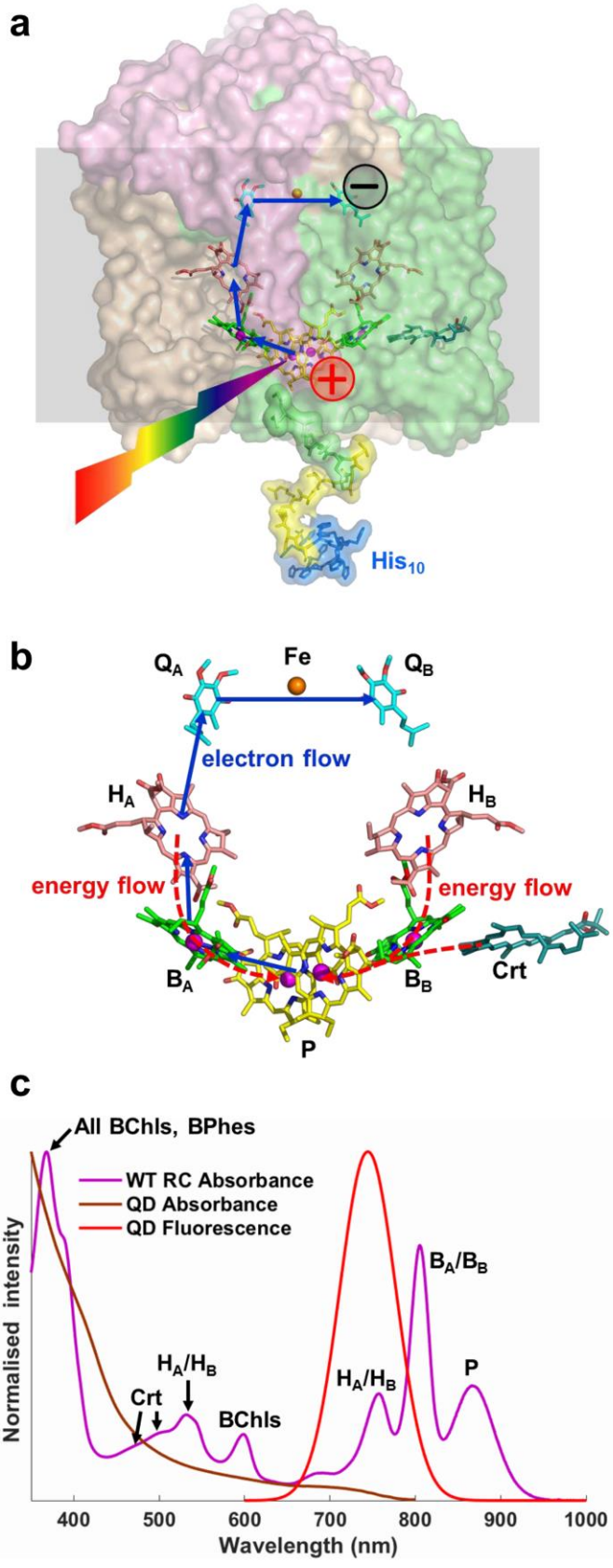
a
His10
b
QA
Fe
QB
electron flow
HA
HB
energy flow
energy flow
BA
BB
Crt
P
c
All BChls, BPhes
WT RC Absorbance
QD Absorbance
QD Fluorescence
Normalised intensity
HA/HB
Crt
BChls
HA/HB
BA/BB
P
400
500
600
700
800
900
1000
Wavelength (nm)

Figure 1. Structure of the RC and optical properties of components. (a) The *Rba. sphaeroides* RC comprises three polypeptides (transparent pink, green and beige surfaces) that scaffold ten cofactors embedded in the interior of the photosynthetic membrane (grey box). Photo-excitation separates charge between BChl and ubiquinone cofactors on opposite sides of the membrane (blue arrows). An engineered extra-membrane deca-histidine tag (blue surface) is connected to the protein by a linker (yellow surface). (b) Excited states formed on the RC BPhe (H_A/H_B – pink carbons)) or monomeric BChl (B_A/B_B – green carbons) cofactors by direct photon absorption or energy transfer from an antenna migrate to the primary electron donor (P) BChl pair (yellow carbons) on a sub-picosecond time scale (red dashed arrows). The resulting P* excited state triggers charge separation to the Q_B ubiquinone (cyan carbons) via B_A, H_A and the Q_A ubiquinone (cyan carbons), according to the scheme $P^* \rightarrow P^+B_A^- \rightarrow P^+H_A^- \rightarrow P^+Q_A^- \rightarrow P^+Q_B^-$ (blue arrows). The single carotenoid cofactor (Crt – teal carbons) can also act as a light harvesting pigment. Other atom colours are: oxygen – red; nitrogen – blue; magnesium – magenta sphere; iron – brown sphere. (c) The chosen CdTe QDs absorb across the visible region and their emission overlaps with the lowest energy RC absorbance bands in the near-IR. Individual RC absorbance bands can be attributed to individual cofactors or groups of cofactors. The band at 760 nm is a composite of the individual absorbance bands of the H_A and H_B BPhes, the band at 800 nm is a composite of the individual absorbance bands of the B_A and B_B BChls, and the band at 870 nm is attributable to the P BChl pair. The carotenoid (spheroidenone) has a broad absorbance band between 450 and 600 nm.

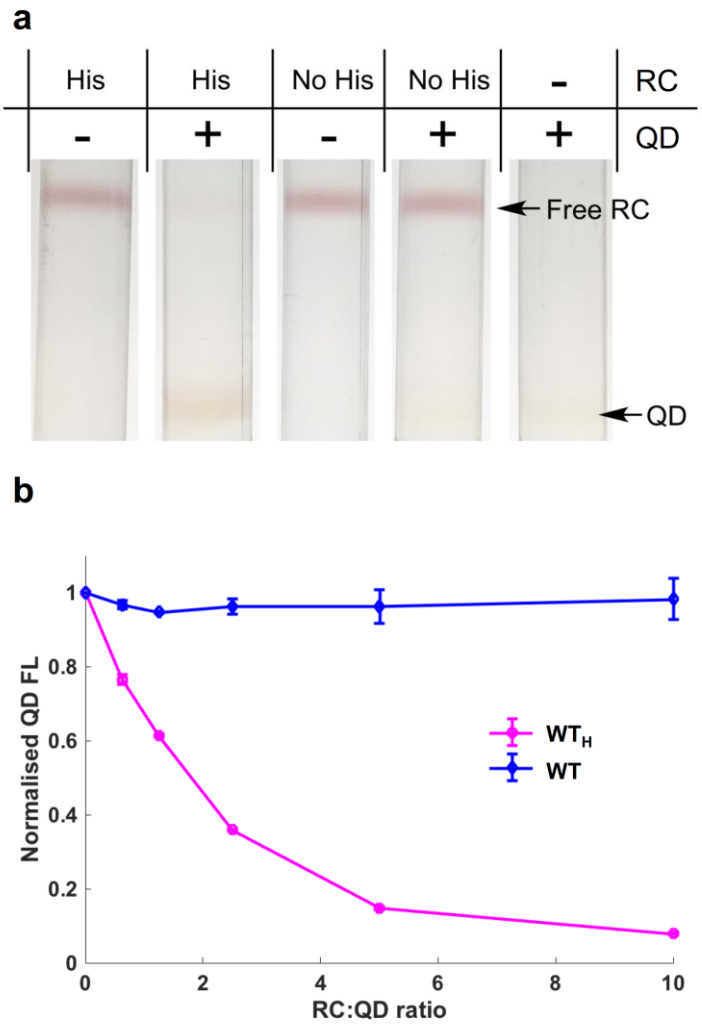

Figure 2. Binding of RCs to QDs and quenching of QD emission. (a) Two-step sucrose gradients that separate unbound RCs (top red band) from QDs or RC/QD conjugates (bottom brown band). (b) Intensities of QD emission at different RC:QD ratios relative to a QD-only control (excitation at 430 nm).

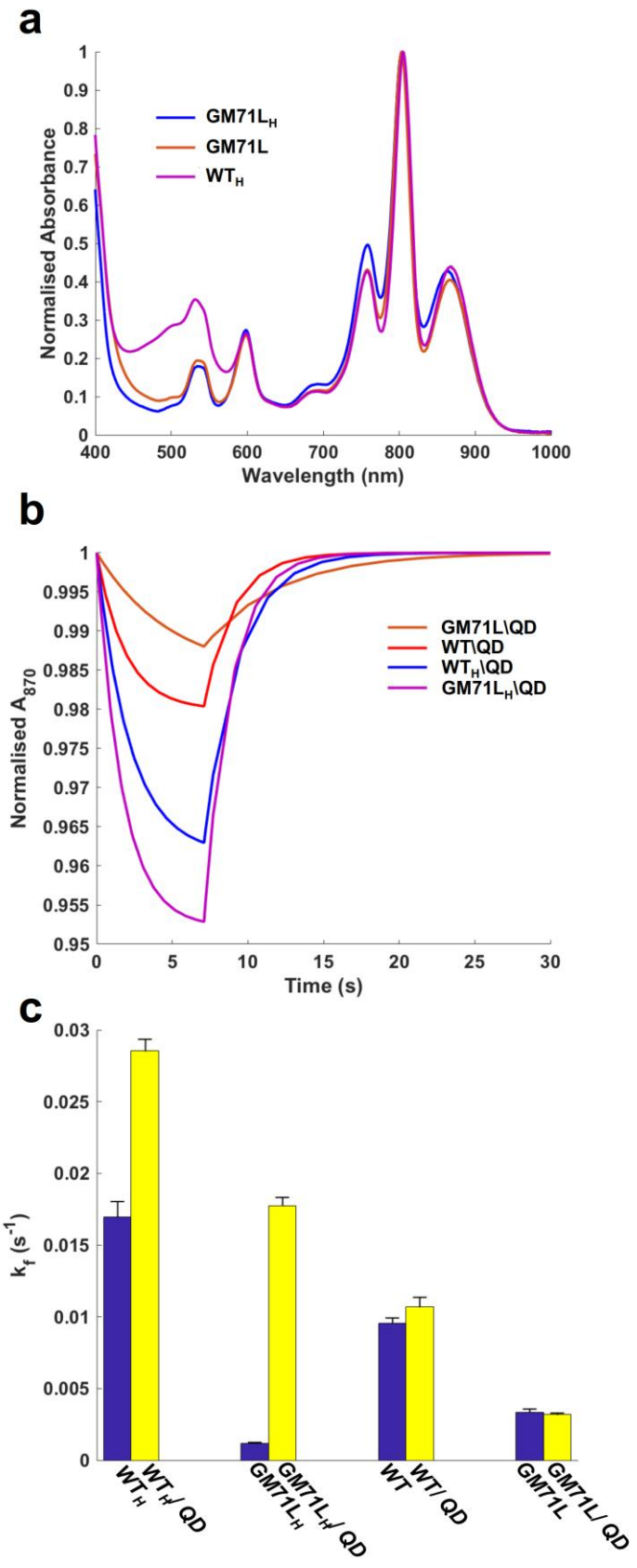
a
Normalised Absorbance
Wavelength (nm)
GM71L$_H$
GM71L
WT$_H$
b
Normalised A$_{870}$
Time (s)
GM71L\QD
WT\QD
WT$_H$\QD
GM71L$_H$\QD
c
k$_f$ (s^{-1})
WT$_H$
WT$_H$/ QD
GM71L$_H$
GM71L$_H$/ QD
WT
WT/ QD
GM71L
GM71L/ QD

Figure 3. Enhanced P photobleaching in QD conjugates relative to unbound RCs. (a) Absorbance spectra. The GM71L and GM71L$_H$ mutant RCs lack the single RC spheroidenone carotenoid which has broad absorbance between 420 and 580 nm. (b) Normalised RC photobleaching at 870 nm in 2.5 RC:QD mixtures of QDs and WT or GM71L RCs with and without a His-tag. Excitation was at 450 nm for 7 seconds. Data shown are fits to averaged kinetic traces (see Figure S2, Supporting Information). (c) Rate constants for photobleaching of P absorbance at 870 nm (k_f). A rate enhancement was seen when WT$_H$ or GM71L$_H$ RCs were conjugated to QDs.

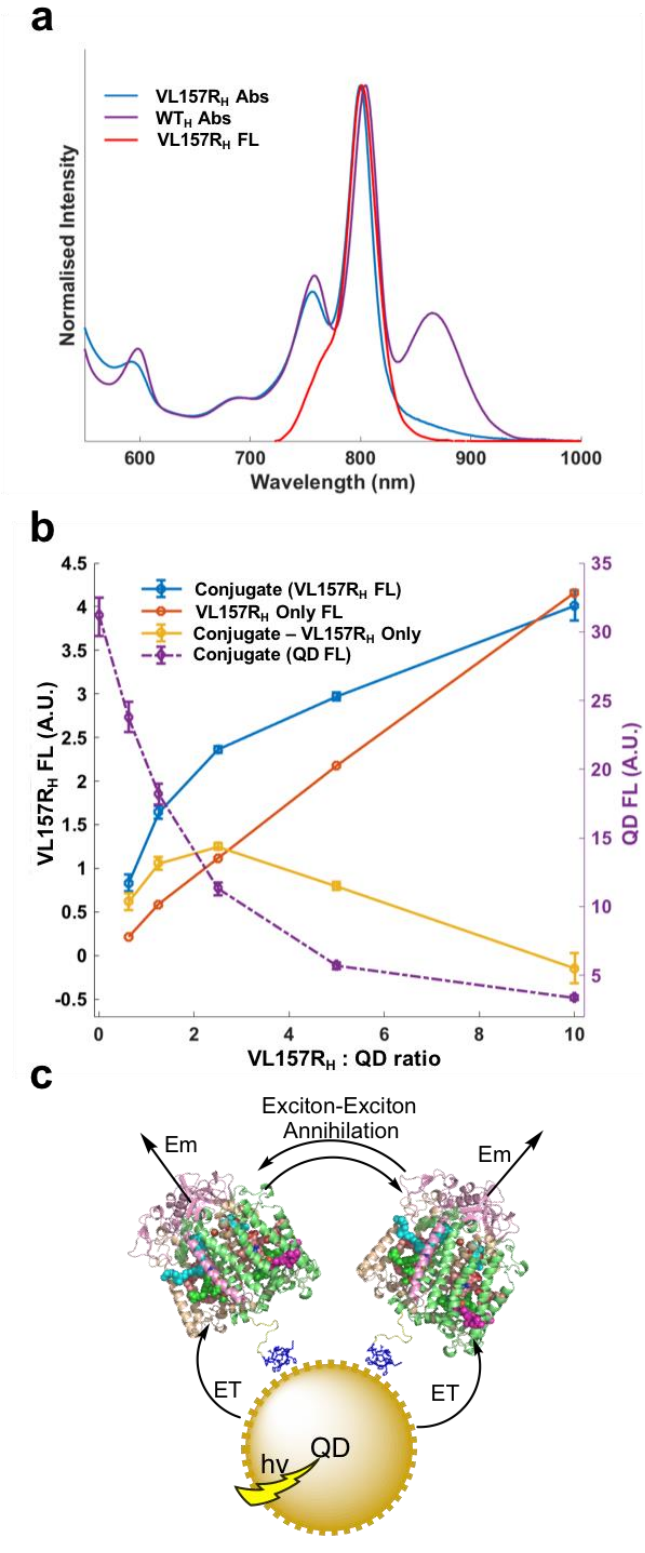
a
VL157R$_H$ Abs
WT$_H$ Abs
VL157R$_H$ FL
Normalised Intensity
600
700
800
900
1000
Wavelength (nm)
b
Conjugate (VL157R$_H$ FL)
VL157R$_H$ Only FL
Conjugate – VL157R$_H$ Only
Conjugate (QD FL)
VL157R$_H$ FL (A.U.)
QD FL (A.U.)
VL157R$_H$: QD ratio
c
Exciton-Exciton
Annihilation
Em
Em
ET
ET
hν
QD

Figure 4. Quenching of QD emission by RCs lacking the P BChls. (a) Absorbance and emission spectra for the VL157R_H RC, compared to the absorbance spectrum of the WT_H RC. Spectra are normalised to the signal maximum around 800 nm. (b) Intensity of emission from VL157R_H RCs or QDs at different VL157R_H RC:QD ratios. (c) Schematic of the system. Bringing RCs with artificially long-lived excited states into close proximity by linkage to a QD could promote exciton-exciton annihilation, accounting for a decrease in relative emission when packing densities are highest.

a

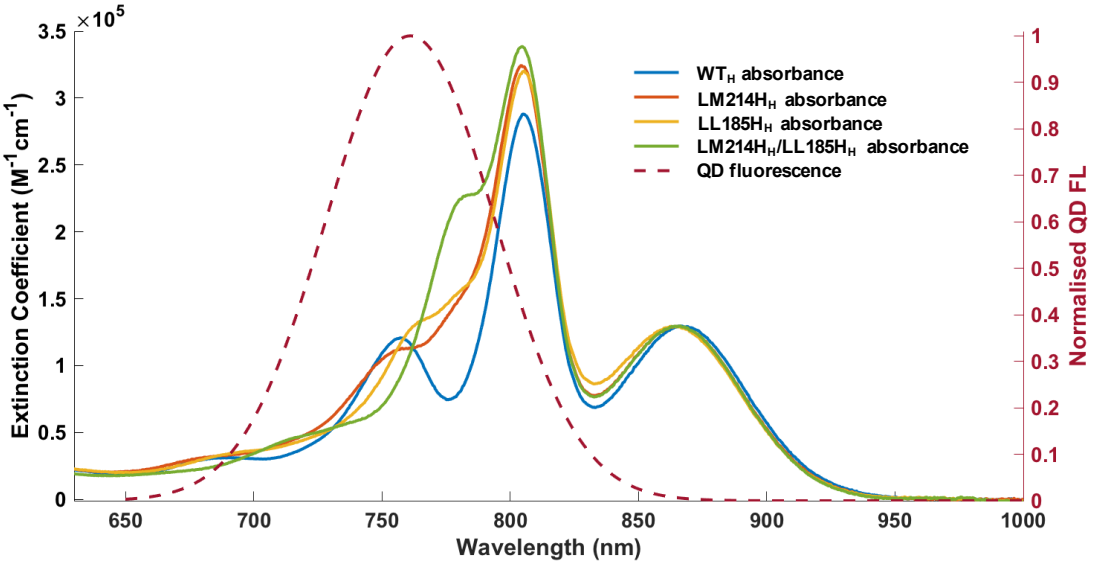

b

RC_H	Spectral overlap J (cm^3M^{-1})
WT_H	3.780×10^{-12}
$LM214H_H$	4.573×10^{-12}
$LL185H_H$	4.546×10^{-12}
$LM214H/LL185H_H$	4.975×10^{-12}

c

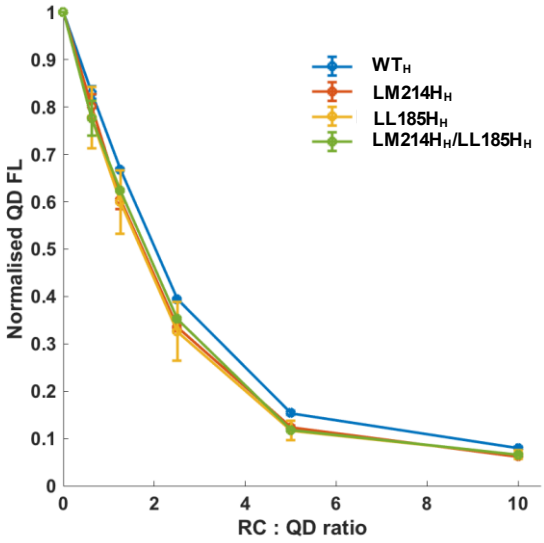

Figure 5. Quenching of QD emission by pigment-exchanged RCs. (a) Absorbance spectra of three His-tagged RCs with single or double BPhe to BChl replacements compared with that of the WT_H RC and the QD emission spectrum. (b) Calculated spectral overlap. (c) Quenching of QD emission at 750 nm as a function of RC:QD ratio (excitation at 430 nm).

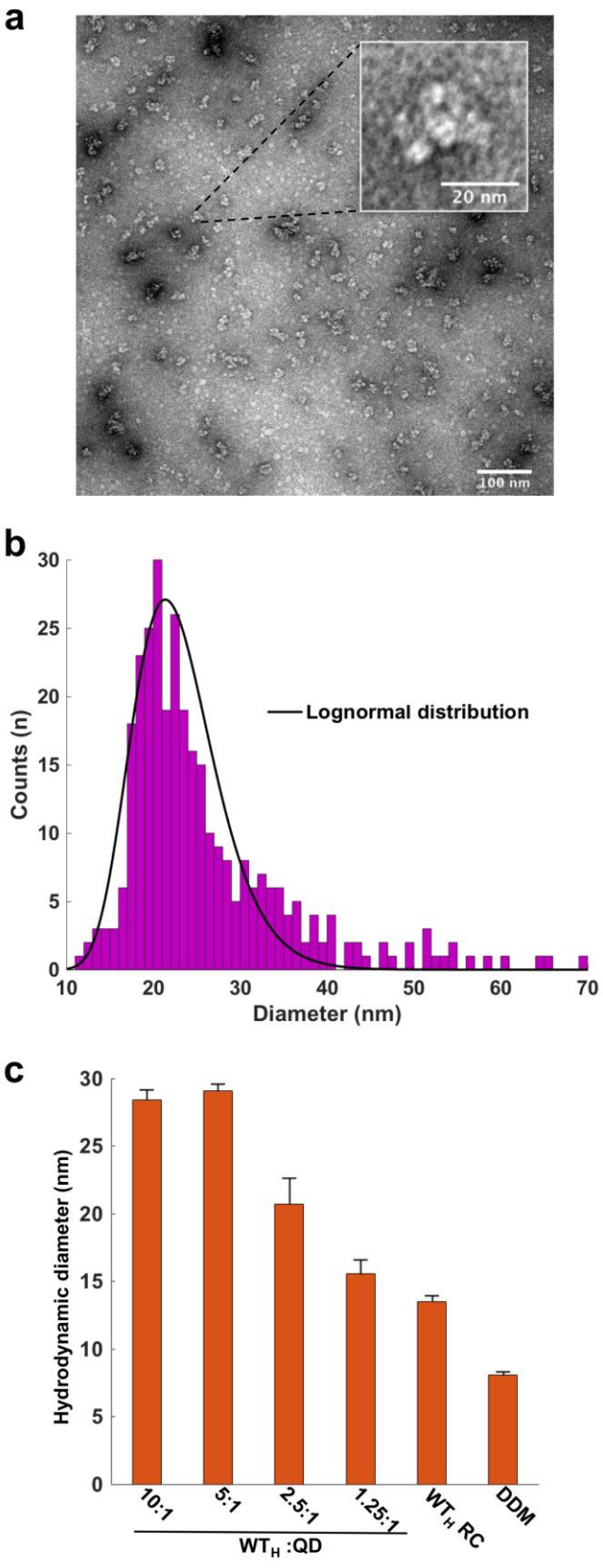
a
20 nm
100 nm
b
Counts (n)
Diameter (nm)
Lognormal distribution
c
Hydrodynamic diameter (nm)
10:1
5:1
2.5:1
1.25:1
WT$_H$ RC
DDM
WT$_H$:QD

Figure 6. Dimensions of RC/QD conjugates. (a) TEM image of RC/QD conjugates formed in 10:1 RC:QD mixture. The inset shows an enlarged view of a typical object, showing multiple clustered bright objects of a dimension consistent with the RC protein. (b) Histogram of object diameter for multiple objects identified by image processing, fitted to a lognormal distribution (mode 21.4 ± 1.0 nm). (c) Hydrodynamic diameters of RC/QD conjugates, WT_H RCs and DDM micelles estimated by DLS (average of 5 measurements with standard deviation).

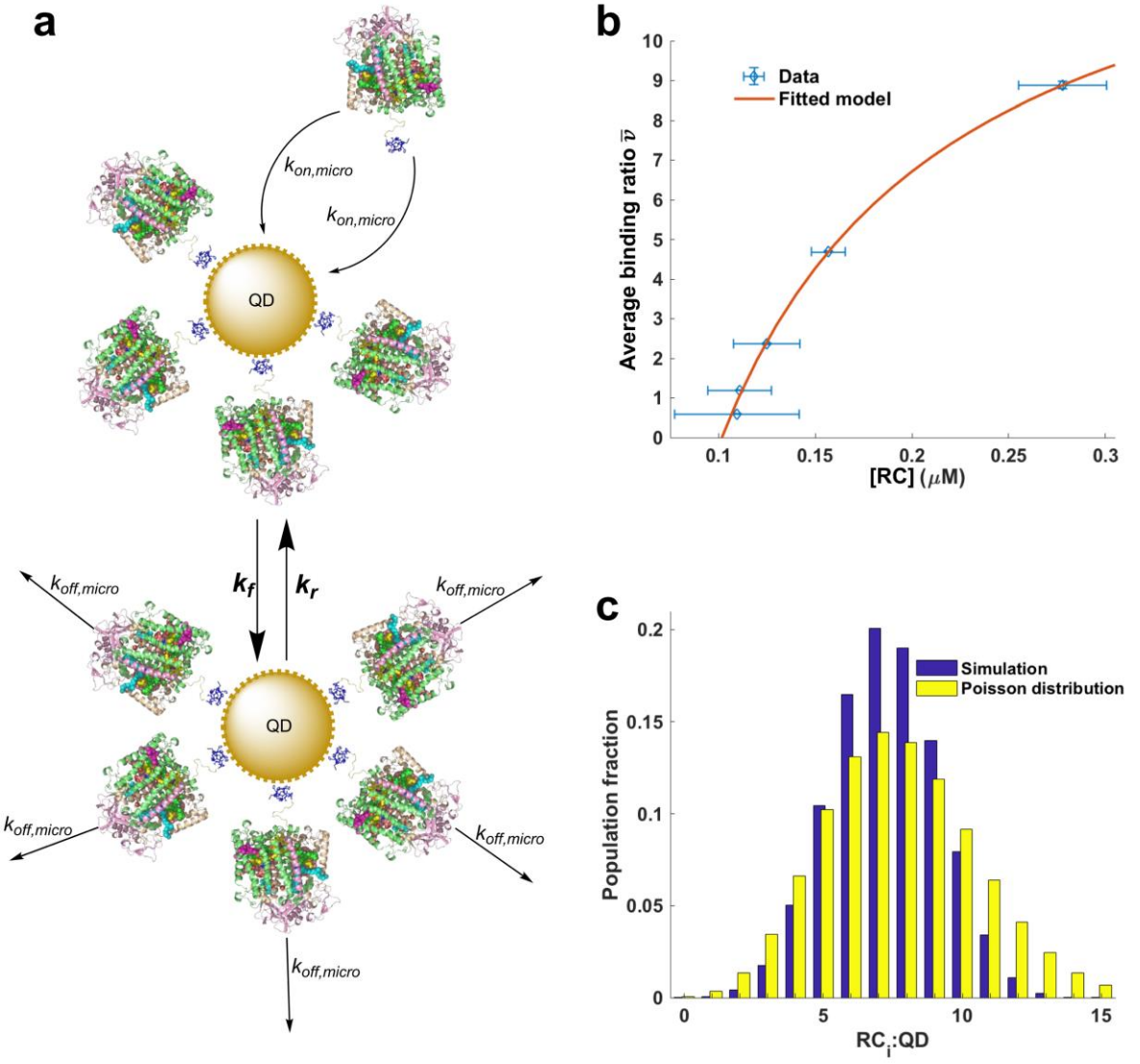

Figure 7. Assessment of distribution in RC:QD stoichiometry. (a) Schematic of model for simulation of binding of His-tagged RCs to multiple equivalent and independent sites on the surface of a QD. (b) Data on average binding ratio as a function of the concentration of unbound RCs fitted using **Equation 2.** (c) Histogram of the fraction of the conjugate population with a certain RC:QD ratio for a mix formed from 10 RCs per QD. The distribution peaked at 7.7 RC per QD with a maximum stoichiometry of 15. A calculated Poisson distribution is shown for comparison.

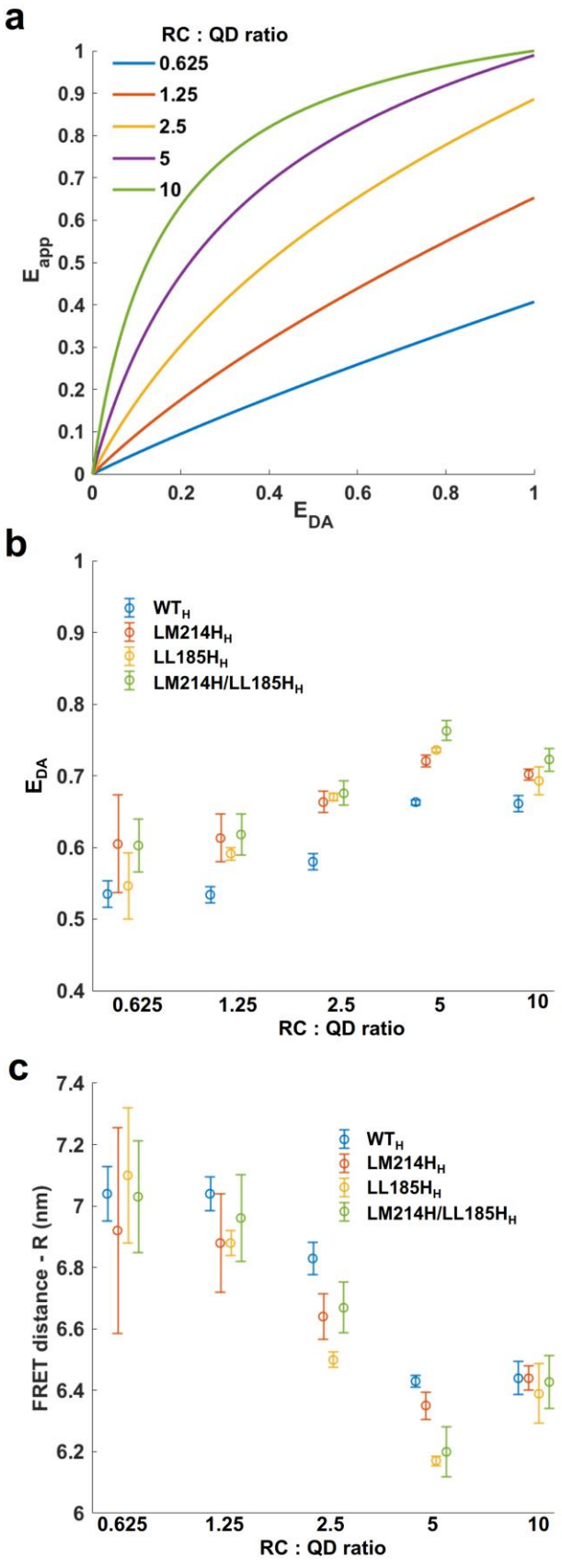
a
RC : QD ratio
0.625
1.25
2.5
5
10
E_app
E_DA
b
WT_H
LM214H_H
LL185H_H
LM214H/LL185H_H
E_DA
RC : QD ratio
c
WT_H
LM214H_H
LL185H_H
LM214H/LL185H_H
FRET distance - R (nm)
RC : QD ratio

Figure 8. Estimations of FRET efficiency and distance. (a) Calculated correlations between the apparent FRET efficiency and the FRET efficiency for a single donor-acceptor pair for different ratios of RC:QD determined using **Equation 7**. (b) Calculated FRET efficiency for a single donor-acceptor pair as a function of RC:QD ratio determined from E_{app} and the correlation in (a). (c) Calculated FRET distance (R) as a function of RC:QD ratio, determined from **Equation 8** and **Equation 9**.

Table of Contents entry:

Nanoconjugates are self-assembled between polyhistidine-modified photosynthetic reaction centers and CdTe quantum dots. The latter act as a synthetic antenna that passes energy to reaction centers by Förster resonance energy transfer and enhances their photochemistry. Modelling this of this tuneable, biohybrid solar energy conversion system provides a thermodynamic description of conjugation that is readily transferable to other conjugate systems.

Keywords: biohybrid, self-assembly, reaction centers, quantum dots, photosynthesis;

Juntai Liu, Judith Mantell, Natalie di Bartolo and Michael R. Jones*

Mechanisms of Self-assembly and Energy Harvesting in Tuneable Conjugates of Quantum Dots and Engineered Photovoltaic Proteins

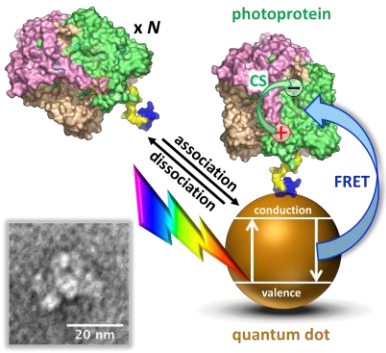

ToC figure

ToC Keyword: Photosynthetic biohybrid